Journal of Medicinal Chemistry

Article

pubs.acs.org/jmc

Dual Targeting of Hypoxic and Acidic Tumor Environments with a Cobalt(III) Chaperone Complex

Natsuho Yamamoto, Anna K. Renfrew, Byung J. Kim, Nicole S. Bryce,* and Trevor W. Hambley*

School of Chemistry, University of Sydney, 412C F11, Sydney 2006, New South Wales, Australia

Supporting Information

ABSTRACT: The rational design of prodrugs for selective accumulation and activation in tumor microenvironments is one of the most promising strategies for minimizing the toxicity of anticancer drugs. Manipulation of the charge of the prodrug represents a potential mechanism to selectively deliver the prodrug to the acidic tumor microenvironment. Here we present delivery of a fluorescent coumarin using a cobalt(III) chaperone to target hypoxic regions, and charged ligands for pH selectivity. Protonation or deprotonation of the complexes over a physiologically relevant pH range resulted in pH dependent accumulation of the fluorophore in colon cancer cells. Furthermore, in a spheroid solid tumor model, the anionic complexes exhibited preferential release of the fluorophore in the acidic/hypoxic region. By fine-tuning the physicochemical properties of the cobalt−chaperone moiety, we have demonstrated selective drug release in the acidic and hypoxic tumor microenvironment.

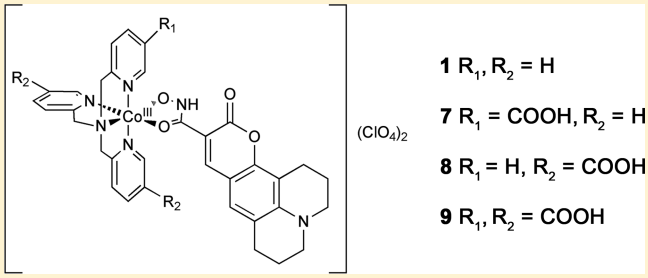

INTRODUCTION

Targeted anticancer prodrugs present a therapeutic opportunity to deliver cytotoxins directly to a solid tumor while minimizing the toxic side effects of active drug exposure. Solid tumors have several unique characteristics, including hypoxia[1] and lower extracellular pH,[2] which can be exploited to allow selective activation of prodrugs.[3,4] The hypoxic and acidic microenvironment within a tumor promotes chemoresistance, radioresistance, and enhanced metastatic potential in a population of cells that are less susceptible to antiproliferative drugs.[5,6] Drug diffusion to the hypoxic region of a tumor is decreased as it is limited by physical properties such as distance from the vasculature and interstitial pressure.[7−9] To be effective, prodrugs that target these difficult to kill tumor cells will need to diffuse throughout the entire tumor, have enhanced cellular uptake in the hypoxic/acidic regions of the tumor, and be selectively activated in these regions.

Cobalt(III) chaperone complexes have been used for hypoxia selective delivery of a number of structurally different drugs, including the MMP inhibitor Marimastat (mmst), DNA minor groove alkylators. and several nitrogen mustards, both in vitro and in vivo.[10−16] Cobalt(III) complexes are highly inert and can form very stable complexes with cytotoxins, deactivating the cytotoxins by coordination and selectively releasing them in hypoxic tumor environments following reduction to labile cobalt(II). Fluorescence tagging of cobalt(III) compounds has proven to be an effective and noninvasive method for monitoring ligand release and the subsequent cellular accumulation and localization of the cytotoxin. We have previously shown that **1**, which contains **2** as a fluorescent mimic of cytotoxic hydroxamic acids (such as Marimastat), and **3** as the ancillary ligand, can be used in live cell imaging as the fluorescence of **2** is strongly quenched when coordinated to a cobalt center, allowing ligand release to be monitored by the return of fluorescence.[16−19]

The extracellular pH in tumor tissues is approximately 0.5 to 1 pH units lower than the extracellular pH in normal tissues, which is sufficient to affect drug uptake.[20−23] In the acidic tumor microenvironment, the protonation of doxorubicin, a weakly basic drug, results in a charged form that has poor cellular accumulation.[24,25] In contrast, the weakly acidic drug chlorambucil, which becomes neutral upon protonation, is known to have improved membrane penetration and cellular accumulation in the acidic extracellular environment of tumors, leading to a degree of tumor selectivity.[21,26] Manipulation of compound charge has been shown to result in pH selective activity of a DNA photocleaver (pH-gating) within an intracellular environment.[27,28] We hypothesized that the rational design of a weakly acidic prodrug with a pK_a around 7 would allow the selective cellular uptake and accumulation of a drug in the acidic tumor microenvironment. Fine-tuning of the physicochemical properties such as the pK_a and charge of the hypoxia selective cobalt(III) chaperone complexes can be achieved by manipulation of the ancillary ligands.[29]

To determine the physicochemical properties required for targeting both hypoxic and acidic tumor microenvironments, a series of cobalt complexes of **2** with charges ranging from +2 through to −2 was synthesized. Increasing numbers of negative charges were incorporated into the complex in the form of

Received: October 10, 2012
Published: November 30, 2012

   dx.doi.org/10.1021/jm3014713 | J. Med. Chem. 2012, 55, 11013−11021

Scheme 1. Synthesis of $[Co(c343haH)(tpa(COOH)_n)](ClO_4)_2$

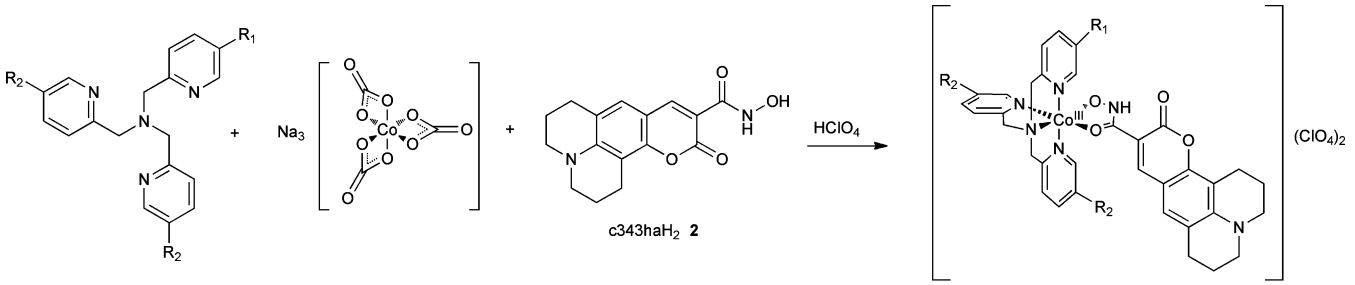

c343haH$_2$ **2**

R_1, R_2 = H: tpa **3**
R_1 = COOH, R_2 = H: tpa(COOH)$_1$ **4**
R_1 = H, R_2 = COOH: tpa(COOH)$_2$ **5**
R_1, R_2 = COOH: tpa(COOH)$_3$ **6**

R_1, R_2 = H: $[Co(c343haH)(tpa)](ClO_4)_2$ **1**
R_1 = COOH, R_2 = H: $[Co(c343haH)(tpa(COOH)_1](ClO_4)_2$ **7**
R_1 = H, R_2 = COOH: $[Co(c343haH)(tpa(COOH)_2](ClO_4)_2$ **8**
R_1, R_2 = COOH: $[Co(c343haH)(tpa(COOH)_3](ClO_4)_2$ **9**

carboxylate groups appended to the nonbinding 3-position of the pyridine rings of **3**. The results show that changing the properties of the complexes in this way greatly impacts on their diffusion, cellular accumulation, and the targeted delivery of the ligand to the hypoxic areas of a 3-dimensional tumor model. Thus, we have generated a novel drug delivery system rationally designed to target chemotherapy-refractive tumor microenvironments by simultaneously exploiting hypoxia and pH.

RESULTS AND DISCUSSION

Syntheses of the Complexes. A series of analogous but differently charged ancillary ligands, **4**, **5**, and **6**, were prepared by introducing negative charges as carboxylate groups on the nonbinding 3-position of the pyridine rings, generating a series with different numbers of nicotinic acid groups (Scheme 1, Table 1). The 3-position was chosen for functionalization in order to minimize steric crowding around the metal center and to prevent coordination of the carboxylate to cobalt. The nicotinic acid groups (pK_a ~4.6)[30] are deprotonated at physiological pH, and therefore each nicotinic acid group will decrease the charge of the complex by one.

Table 1. The Charges of the Ligands and That of the Corresponding Cobalt Complexes in Different pH Environments

ligand		**3**	**4**	**5**	**6**
charge		0	−1	−2	−3
complex	**2**	**1**	**7**	**8**	**9**
pK_a	8.3	5.6	6.6	7.5	7.7
charge					
pH 6.0	0	+1.3	+0.8	0	−1.0
pH 7.4	−0.1	+1.0	+0.1	−0.4	−1.3

All of the complexes were successfully synthesized using a simple one-pot procedure (Scheme 1) and characterized by mass spectrometry and elemental analysis. The elemental analysis results show that the complexes were all isolated in the hydroxamate form with the carboxylates protonated as the complexes were found to have a 2+ charge, as indicated by the presence of two ClO_4^- counteranions.

Initial ^{1}H NMR studies of the complexes revealed very broad and indistinct peaks (Supporting Information Figure S1a). This was thought to be due to either exchange between the hydroxamate/hydroximate forms or the presence of isomers. Previously conducted ^{1}H NMR studies of cobalt−tpa complexes with hydroxamates, such as Marimastat, have shown that isomers (*cis*- and *trans*- with respect to the disposition of **3** relative to the hydroxamate) exist in roughly a 1:1 ratio in solution.[15] Furthermore, the lower symmetry of ligands **4** and **5** was expected to give rise to an additional two isomers (*S*- and *U*-) of complexes **7** and **8**. By acidifying the solution to pH 3, such that all of the complexes were in the hydroxamate form, well resolved ^{1}H NMR spectra could be obtained (Supporting Information Figure S1b−d). These spectra confirmed the presence of the *cis*- and *trans*- isomers of the hydroxamic acid for each complex as well as the *S*- and *U*- isomers of complexes **7** and **8**. It was not possible to separate these isomers by preparative HPLC as the complexes were not stable under the conditions required for HPLC. However, as the outcome of the studies was not expected to be affected by the different isomers, the complexes were used as mixtures.

The cobalt−fluorophore complexes all have highly negative cathodic peak potentials close to −1000 mV (vs NHE) due to the electron withdrawing effects of the hydroxamate moiety (Table 2). The electron-withdrawing carboxylate groups of the nicotinic acids reduce the stability of the Co(III) state, resulting in complex **9**, which has the most nicotinic acid ligands, having the most positive cathodic peak potential.

Table 2. Cathodic Peak Potentials[a]

complex	E_p vs Ag/AgCl in H_2O (mV)	E_p vs fc/fc+ in DMF (mV)	E_p vs NHE (mV)
1[17]	not measured	−1968	−1288
7	not measured	−1856	−1136
8	−1278	not measured	−1080
9	−1156	not measured	−958

[a]Values given vs NHE are calculated using redox values of $[Fe(\eta^5\text{-}C_5H_5)_2]^{0/+}$ = +0.72 V vs NHE in DMF[44] and Ag/AgCl, KCl (saturated) = +0.198 vs NHE at 25 °C.[45]

Determination of the Hydroxamic Acid Amine pK_a. For pH-dependent cellular accumulation of a cobalt prodrug to occur, it is necessary that the charge of the complex change over the pH range encompassed by normal and tumor tissues (pH 6−7.4). The pK_a value of the hydroxamic acid amine of free c343haH$_2$ is 8.3,[31] higher than the pH relevant range. The pK_a values of the complexes **1**, **7**, **8**, and **9** were determined by UV−vis titration (Table 1 and Supporting Information Figure

dx.doi.org/10.1021/jm3014713 | J. Med. Chem. 2012, 55, 11013−11021

S2) and found to be 0.6−2.7 pH units lower than that of the free ligand. The values increase with the number of electron-withdrawing groups on the ancillary ligand, as observed for related Co(III) complexes.[32]

These pK_a values indicate that the proportions of the differently charged species will differ in the slightly basic extracellular pH of normal tissue and the acidic extracellular environment of tumors (Table 1), allowing pH selective accumulation. For complexes **1** and **7**, the positive charge of the complexes will increase in the acidic extracellular environment of tumors. However, complexes **8** and **9** by virtue of their negative charges will exist with charges close to neutral in the acidic regions of the tumor.

Fluorescence Quenching and Recovery. The fluorescence of the complexes is significantly quenched (98−99%) relative to that of the free fluorophore (Figure 1a) as previously observed for complex **1**.[17] Importantly, for quantitative fluorescence microscopy measurements, the fluorescence intensity of the free fluorophore and the complexes is not pH dependent in the pH range of 2−10 (Supporting Information Figure S3).

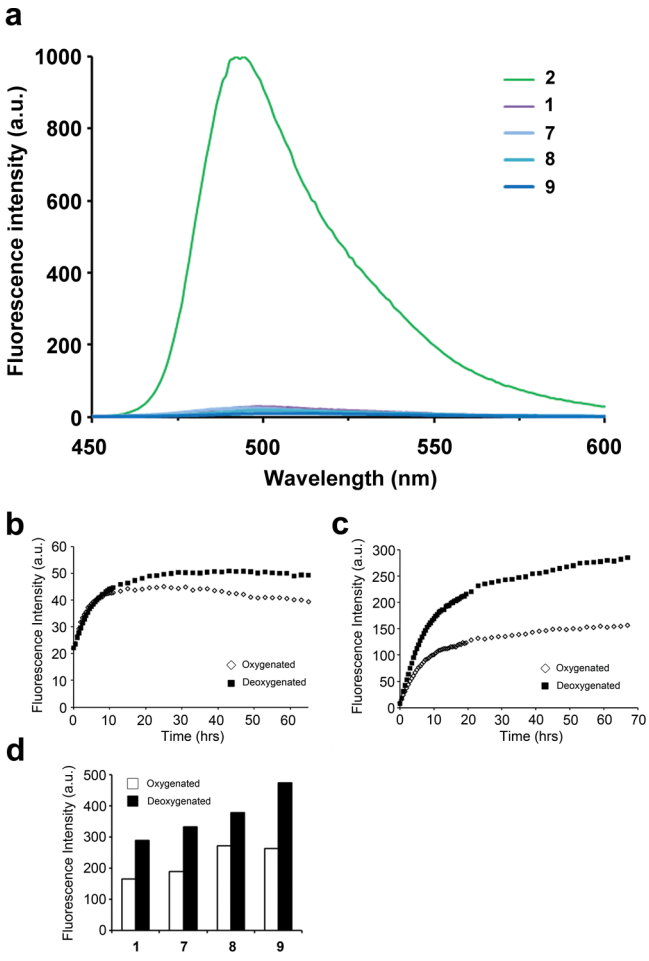

Figure 1. (a) Fluorescence emission spectra of 70 μM solutions of the free fluorophore and the fluorophore complexes. (b) and (c) Fluorescence return of oxygenated and deoxygenated solutions of **1** and **9** in the presence of ascorbic acid. (d) End-point fluorescence intensities of the fluorophore complexes treated with ascorbic acid in oxygenated and deoxygenated solutions at pH 7.5.

To investigate the extent of activation of the complexes by cellular reductants, **1**, **7**, **8**, and **9** were treated with ascorbic acid in both oxygenated and deoxygenated solutions (basified to pH 7.5 by addition of 1 M NaOH) and the fluorescence emission spectra monitored over 70 h (Figures 1b−d). Negligible increase in fluorescence was observed in solutions of the complexes without ascorbic acid treatment over the same time period. Activation of the complexes was evident from the increase in fluorescence intensity owing to release of **2**. For each complex, a greater rate and extent of fluorescence return was observed in the deoxygenated solution, suggesting that activation is enhanced by hypoxic conditions and that the activation occurs via reduction to Co(II) rather than ligand exchange in the Co(III) state. A correlation can be drawn between the extent of oxygen dependent fluorescence increase and the cathodic peak potential. Complex **1**, which has the most negative cathodic peak potential, also shows relatively little fluorescence return, whereas complex **9**, which has the most positive cathodic peak potential, shows the greatest amount of fluorescence return. This is consistent with a reductive mechanism of activation and reveals that a small decrease in the stability of the Co(III) state can have a substantial effect on the rate and extent of reduction by ascorbate.

Complex Charge and Cytotoxicity. The cytotoxicity of each of the complexes and the free c343haH ligand were evaluated in the human colorectal carcinoma cell line DLD-1. The cobalt−tpa chaperones moieties did not significantly affect the cytotoxicity of the free ligand, with IC_{50} values found to be within 40 and 58 μM (Supporting Information Table S1). Importantly, neither the free ligand nor the complexes are significantly cytotoxic at the concentrations required for cellular uptake and distribution experiments.

pH Dependent Cellular Accumulation of Charged Cobalt−Fluorophore Complexes. Cellular accumulation of the cobalt complexes in the human colorectal cancer cell line DLD-1 was determined using cobalt uptake and fluorescence microscopy. Figure 2c shows the cobalt uptake in cells treated with the cobalt−fluorophore complexes at pH 7.4. For all complexes, the cobalt concentration is significantly above background, with the neutral complex **7** showing the highest cellular accumulation of cobalt. To evaluate the influence of pH on cobalt uptake, the accumulation study was repeated at pH 6; however, negligible cobalt was found in cells treated with the complexes. Acidic environments in tumor cells are known to strongly increase drug efflux rates[33] and efflux of the cobalt product following release of the c343ha would explain the low levels of cobalt observed and the high levels of c343haH generated fluorescence.

Using fluorescence microscopy, release of the c343haH ligand from the cobalt complexes and subsequent cellular accumulation of the free ligand was examined over a range different extracellular pH values. As expected from their pK_a values, the accumulation of the free fluorophore **2** was consistent across the whole pH range whereas the cobalt−fluorophore complexes exhibit pH dependent trends in accumulation as shown by the fluorescence intensity in cells at the tested pH values (Figure 2a,b). pH does not affect the fluorescence intensity of **2** (Supporting Information Figure S3), suggesting that pH dependent fluorescence observed in cells treated with the cobalt−fluorophore complexes **1**, **7**, **8**, and **9** is the result of pH dependent cellular accumulation of the complexes followed by intracellular release of the fluorophore.

dx.doi.org/10.1021/jm3014713 | J. Med. Chem. 2012, 55, 11013−11021

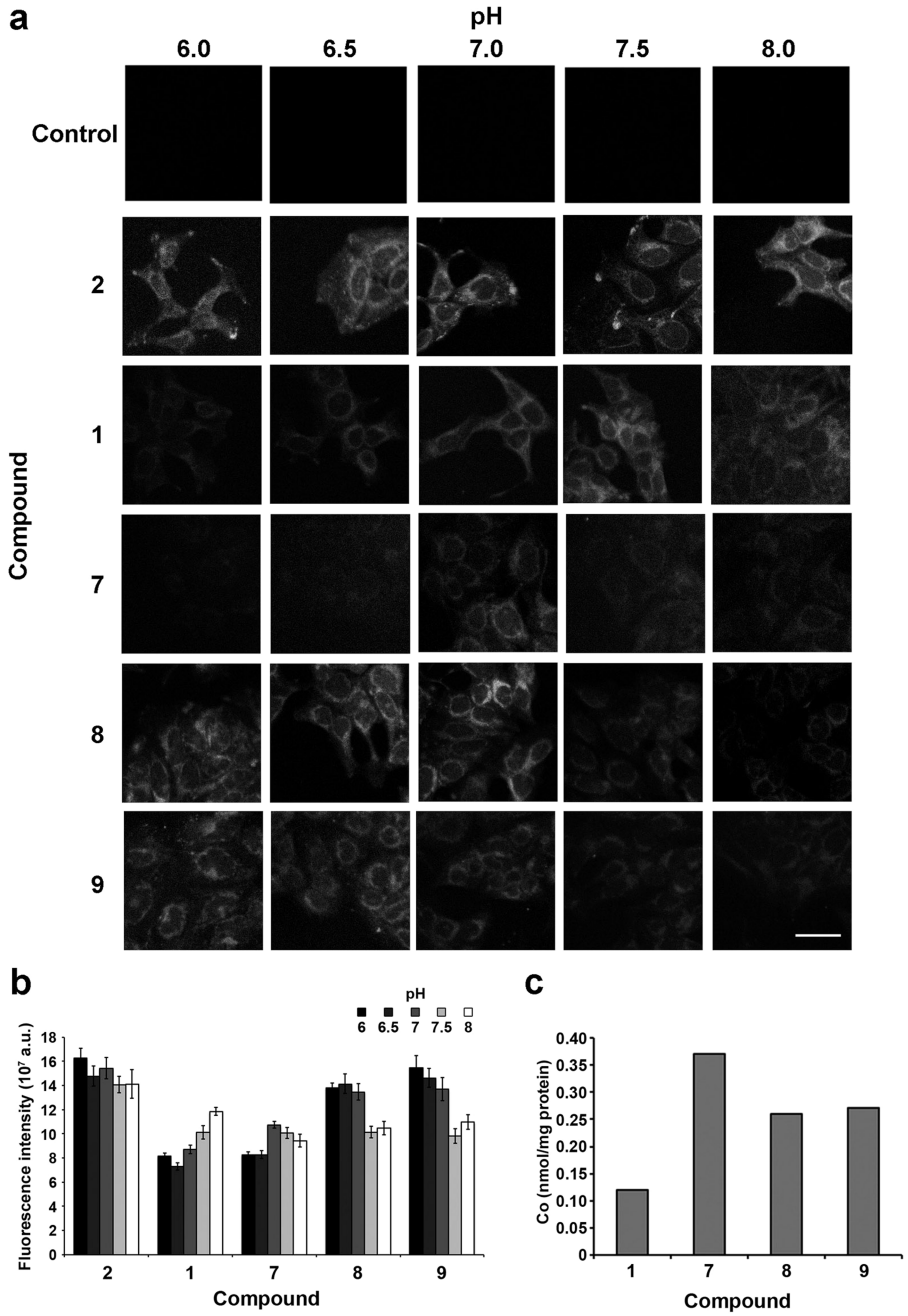

Figure 2. Cellular uptake is dependent on the charge of the compound and pH of the environment in monolayer cells. (a) Confocal microscopy images of pH-adjusted DLD-1 cells after treatment with the fluorophore complexes for 4 h. Scale bar represents 20 μm. (b) Quantification of the fluorescence intensities in Figure 3a. (c) Cellular uptake of cobalt in DLD-1 cells treated with the fluorophore complexes.

This observation is in agreement with the high levels of cellular cobalt.

For each complex, a clear correlation between calculated charge and cellular accumulation was observed. Charged complexes do not easily penetrate the cell membrane,[34,35] therefore, the complexes are expected to exhibit the highest accumulation where their charge is closest to neutral. Complexes **1** and **7** have increasingly positive charges at more acidic pH and should exhibit greater accumulation at higher pH values. Complex **1** shows a clear increase in fluorescence intensity at more basic pH values, with the intensity at pH 8 being 2-fold greater than that at pH 6. For complex **7**, the influence of pH on uptake is less marked; however, fluorescence intensity increases between pH 6 and pH 7.

Complexes **8** and **9** are expected to exhibit better accumulation at more acidic pH values where they are less negatively charged. Both complexes show a similar trend in pH dependent uptake, with a gradual decrease in fluorescence intensity from pH 6 to pH 8. The two complexes exhibited similar levels of both cobalt and c343haH accumulation at all pH values tested. This result is unexpected as **9** is negatively charged across the whole pH range and would be expected to show very little cellular uptake. A possible reason for this is that one of the nicotinic acid groups is transiently protonated in the tumor microenvironment, which would result in the complex being neutral. The first pK_a of the nicotinic acid groups in

dx.doi.org/10.1021/jm3014713 | J. Med. Chem. 2012, 55, 11013−11021

complex **9** is approximately 4.8, meaning that 5% would be protonated at pH 6 and 1% at pH 7.5. It is to be expected that **9** exists in an equilibrium in which the majority of the complex is negatively charged but a small percentage is neutral, with cellular uptake of the neutral complex resulting in an equilibrium shift toward the protonated form in the extracellular media.

Complexes **8** and **9** exhibit higher average fluorescence intensities than **1** and **7**. This observation is in agreement with the fluorescence return studies, which suggest that in the presence of reducing agents, the fluorophore ligand is released more rapidly from complexes **8** and **9** than **1** and **7**. The intensity of fluorescence observed in cells is therefore likely to be a function of both cellular uptake and the rate of fluorophore release from the complexes.

Selective Uptake and Activation of the Cobalt(III) Complexes in the Acidic and Hypoxic Region of Solid Tumor Models. Spheroids are three-dimensional aggregates of tumor cells that display many of the characteristics of solid tumors, including concentration gradients of oxygen and biochemical waste products, areas of hypoxia and necrosis, and similar drug diffusion profiles.[16,36,37] To determine the effectiveness of these complexes as pH and hypoxia selective agents in a three-dimensional tumor model, genetically modified DLD-1 cells that fluoresce when experiencing hypoxia[16] were grown as spheroids, treated with the complexes, and the distribution of fluorescence visualized. The images in Figure 3 show the blue fluorescence due to the free fluorophore **2** (Figure 3a) or the fluorophore released from the complex (Figures 3b–e) simultaneously with the red fluorescence generated by cells in hypoxic regions. The spheroids treated with the free fluorophore **2** only showed fluorescence in the periphery, indicative of limited diffusion. Spheroids treated with the complexes showed a ring of fluorescence at the periphery and a central region of florescence that overlapped with the fluorescent hypoxic cells.

When quantified, the fluorescence intensity observed in the acidic, central regions of the spheroids was found to increase with the numbers of nicotinic acid ligands on the complex (Figure 3f). Least fluorescence was observed toward the center of the spheroids treated with complex **1**, with significantly more fluorescence observed in spheroids treated with the single and dual carboxylate containing complexes **7** and **8**. Complexes **8** and **9** show greater accumulation in the hypoxic and necrotic regions of the spheroids.

The higher fluorescence observed in the hypoxic regions of the spheroids treated with complexes that have more nicotinic acid groups suggests that these complexes penetrate further into and/or are being activated to a greater extent in the hypoxic regions of the spheroid. Both are possible: the increased penetration is in accord with the negatively charged complexes traveling further into the core of the spheroid because they are less likely to be sequestered into cells closer to the surface. The greater extent of activation is in accord with the less negative cathodic peak potentials and the increased tendency for these complexes to undergo hypoxia-enhanced activation.

Close inspection of Figure 3d,e reveals that treatment with complex **8** results in the bulk of the blue fluorescence being closely coincidental with the red fluorescence of the hypoxic region whereas treatment with complex **9** results in the bulk of the blue fluorescence lying at the very center of the spheroid. This region is believed to be populated by a high proportion of necrotic cells, and we have observed accumulation in this region of compounds that are taken up very slowly by cells.[36] This is consistent with the negative charge on complex **9** slowing cellular uptake to the extent that it penetrates to this region where it is trapped and suggests that, as expected, the properties of complex **8** are optimal for targeting the hypoxic region.

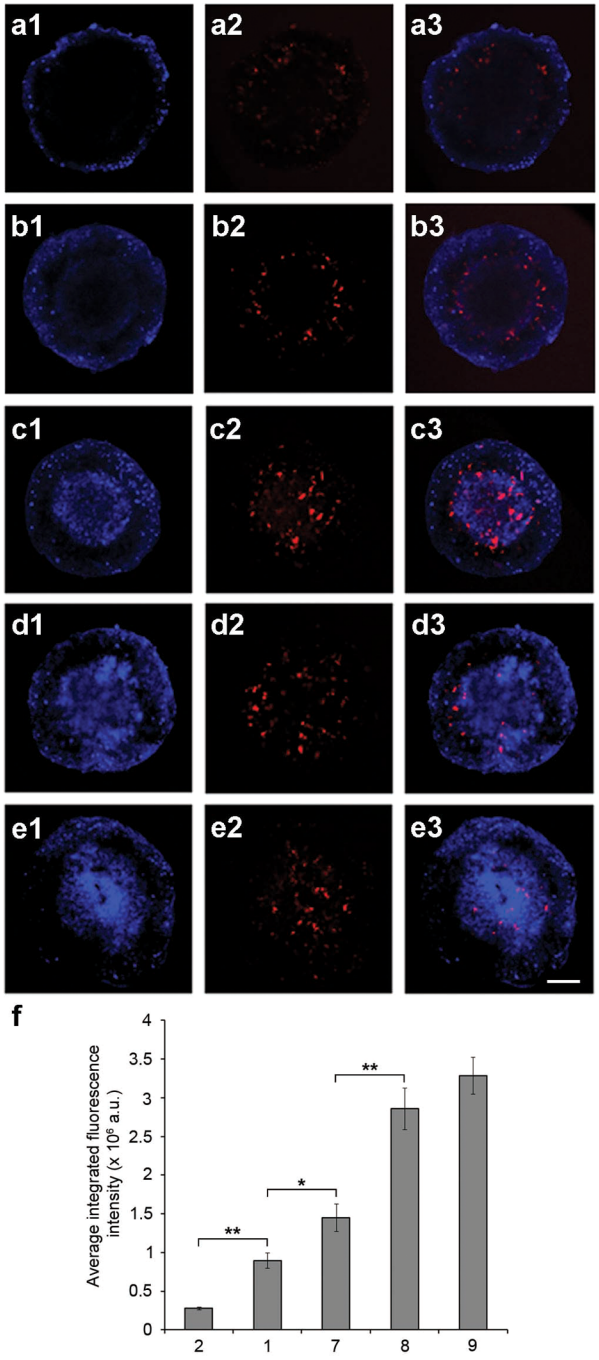

Figure 3. Uptake of the complexes in spheroids is dependent on the charge of the compound. Confocal microscopy images of HRE-Eos DLD-1 spheroids treated with (a) free fluorophore **2**, (b) complex **1**, (c) complex **7**, (d) complex **8**, and (e) complex **9**. Column 1 shows the fluorescence due to the ligand in the blue channel, column 2 shows the cellular expression EosFP in response to hypoxia in the red channel, and column 3 shows the overlay. Scale bar represents 200 μm. (f) Quantification of the fluorescence intensities in (a1–e1). $^{*}P < 0.005$ and $^{**}P < 0.001$ compared to the preceding treatment group.

dx.doi.org/10.1021/jm3014713 | J. Med. Chem. 2012, 55, 11013–11021

For complexes **8** and **9**, it is assumed that the hydroxamic acid amine is deprotonated and therefore the complexes have a higher charge at neutral pH. However, when they reach the acidic core of the spheroids, the hydroxamic acid amine is more likely to become protonated and the complexes are expected to become neutral or close to neutral so that cellular uptake can occur more readily. The complexes subsequently undergo activation, but whether this occurs by ligand exchange or reduction is not clear. In the fluorescence return experiments, activation of the complexes by ascorbic acid was found to be enhanced under hypoxic conditions. This hypoxia-enhanced return of fluorescence correlates with the cathodic peak potential, and pattern of fluorescence in the spheroids.

CONCLUSIONS

The results described in this study have demonstrated the effectiveness of the strategy of a small-molecule chaperone prodrug that allows both selective uptake and release of a drug in the most malignant and difficult to treat tumor regions. The series of hydroxamic acid complexes synthesized with ligands with different numbers of nicotinic acid groups demonstrated pH dependent accumulation by tumor cells and excellent penetration into solid tumor models. These are highly promising results, which demonstrate that both hypoxia and pH selectivity can be achieved by fine-tuning the reduction potentials and charges of the chaperone complexes, allowing tight control of cellular accumulation of a cytotoxin in both monolayer cell culture and spheroids. While these results have focused on the model cytotoxin c343haH, this ligand could easily be replaced with a number of cytotoxic hydroxamic acids such as Marimastat and the histone deacetylase inhibitors Vorinostat, Pabinostat, and Belinostat.[38] The targeted delivery achieved using these model complexes is an encouraging outcome and demonstrates their potential for use as chaperones to deliver anticancer cytotoxins to the most malignant and difficult to treat tumor regions.

EXPERIMENTAL SECTION

Synthetic Protocols. All chemicals and solvents were reagent grade and were used without further purification unless otherwise specified. Syntheses of **1**, **2**, **3**, 6-(hydroxymethyl)nicotinate, methyl 6-(bromomethyl)nicotinate, **12**, and **14** were carried out as described in the literature.[17,39−43]

Synthesis of Dimethyl 6,6′-(Pyridin-2-ylmethylazanediyl)-bis-(methylene)dinicotinate (tpa(COOMe)$_2$) 13. Methyl 6-(bromomethyl)nicotinate (0.298 g, 1.3 mmol) was suspended in 3 mL of THF. To this, 2-picolylamine (85 μL, 89 mg, 0.82 mmol) and DIPEA (300 μL, 222 mg, 1.7 mmol) were added and the mixture was stirred for 3 days. A pinkish precipitate formed, which was removed by filtration. The filtrate was evaporated to dryness in vacuo, and the residue was purified by column chromatography (neutral alumina, 1 cm × 20 cm, 1% MeOH in $CHCl_3$, R_f = 0.38). The combined fractions were evaporated to dryness to yield a brown oil (yield: 0.146 g, 0.36 mmol, 44%). ^{1}H NMR ($CDCl_3$): δ 9.10 (s, 2H, pyridyl), 8.52 (s, 1H, pyridyl), 8.24−8.20 (d, *J* = 8.1 Hz, 2H, pyridyl), 7.65−7.62 (d, *J* = 8.0 Hz, 2H, pyridyl), 7.49−7.46 (d, *J* = 7.8 Hz, 1H, pyridyl), 7.14−7.12 (d, *J* = 7.7 Hz,1H, pyridyl), 3.93 (s, 4H, 2 × CH_2), 3.90 (s, 6H, methyl), 3.87 (s, 2H, CH_2). Mass spectrometry (ESI positive ion): *m*/*z* 406.73 ([tpa(COOMe)$_2$] + H^+).

General Method for Methyl Ester Hydrolysis of (tpa-(COOMe)$_n$). The following describes the methyl ester hydrolysis of **12** to yield **4**, but the general procedure was also applied to **14** and **13** to yield **5** and **6**, respectively. **12** (0.62 g, 1.8 mmol) was dissolved in MeOH (2 mL), and a solution of aqueous KOH (2 M, 1.4 mL) was added. The mixture was stirred at room temperature for 2 h and neutralized with aqueous HCl (1 M, 3 mL). The solution was evaporated to dryness in vacuo, and the residue was dissolved in MeOH. Any undissolved white solid (KCl) was removed by filtration. The filtrate was evaporated to dryness to yield a beige fluffy solid (yield: 0.59 g, 1.8 mmol, quantitative). ^{1}H NMR (MeOD): δ 9.15 (s, 1H, α-pyridyl), 8.85−8.82 (d, *J* = 8.3 Hz, 2H, pyridyl), 8.38−8.33 (m, 4H, pyridyl), 7.98−7.81 (d, *J* = 8.0 Hz, 4H, pyridyl), 7.59−7.55 (d, *J* = 8.1 Hz, 1H, pyridyl), 5.00 (s, 4H, 2 × CH_2), 4.53 (s, 2H, CH_2). Mass spectrometry (ESI negative ion): *m*/*z* 332.87 ([tpa(COO)$_1$]$^-$).

6,6′-(Pyridin-2-ylmethylazanediyl)bis(methylene)dinicotinic Acid (tpa(COOH)$_2$) 5. Yield: 0.132 g, 0.35 mmol, 97%. ^{1}H NMR (MeOD): δ 9.15−9.14 (s, 2H, pyridyl), 8.70−8.69 (d, *J* = 8.4 Hz, 2H, pyridyl), 8.50−8.45 (td, *J* = 8.0 Hz,1H, pyridyl), 8.09−8.02 (d, *J* = 8.0 Hz,1H, pyridyl), 7.92−7.89 (d, *J* = 8.4 Hz, 2H, pyridyl), 4.45 (s, 2H, CH_2), 4.39 (s, 4H, 2 × CH_2). Mass spectrometry (ESI negative ion): *m*/*z* 376.87 ([tpa(COOH)(COO)]$^-$).

6,6′,6″-Nitrilotris(methylene)trinicotinic Acid (tpa(COOH)$_3$) 6. Yield: 0.171 g, 0.40 mmol, 95%. ^{1}H NMR (D_2O): δ 9.10 (s, 3H, pyridyl), 8.60−8.57 (d, *J* = 8.2, 3H, pyridyl), 7.82−7.80 (d, *J* = 8.3 Hz, 3H, pyridyl), 4.47 (s, 3 × 2H, CH_2). Mass spectrometry (ESI negative ion): *m*/*z* 421.80 ([tpa(COOH)$_2$(COO)]$^-$).

General Method for Synthesis of Cobalt Complexes. The following describes the general synthesis of the complexes, followed by the specific method of purification and characterization information for individual complexes. All steps in the procedures containing c343haH$_2$ were carried out in the absence of light. All synthesized complexes were determined to be ≥95% pure by elemental analysis.

$Na_3[Co(CO_3)_3]$ (0.111 g, 0.36 mmol) and c343haH$_2$ (0.113 g, 0.38 mmol) were suspended in (1:1) MeOH:H_2O (20 mL) and stirred on ice for 1 h. To this, 2 drops of 70% aqueous $HClO_4$ were added, giving a pH of approximately 5, and the mixture was stirred for a further 1 h on ice. The suspension turned a green−yellow color, and tpa-(COOH)$_n$ (0.36 mmol) dissolved in 1 mL of MeOH was added dropwise. The mixture was stirred at room temperature overnight, and the solution turned an orange−brown color with the formation of a precipitate.

Synthesis of [Co(c343haH)(tpa(COOH)$_1$)](ClO$_4$)$_2$·1.5H$_2$O 7. The precipitate was collected by suction filtration to give a brown solid that was washed with a small amount of ice-cold H_2O and excess Et_2O, then recrystallized from hot EtOH (yield: 65%). Mass spectrometry (ESI positive ion): *m*/*z* 691.05 ([Co(c343haH)(tpa-(COO)$_1$)]$^+$), 346.07 ([Co(c343haH)(tpa(COOH)$_1$)]$^{2+}$). Elemental analysis required for $C_{37}H_{33}Cl_2CoN_6O_{15.5}$: C, 45.82%, H, 3.84%, N, 9.16%. Found: C, 45.81%, H, 3.63%, N, 9.23%.

Synthesis of [Co(c343haH)(tpa(COOH)$_2$)](ClO$_4$)$_2$·4H$_2$O 8. The precipitate was collected by suction filtration to give a brown solid that was washed with a small amount of ice-cold MeOH and excess Et_2O. This was dissolved in H_2O (70 mL), acidified to a pH of 4 with 1 M aqueous $HClO_4$, then washed with 3 × 100 mL DCM. The aqueous fraction was evaporated to dryness and then recrystallized from hot MeOH to yield an orange−brown solid (yield: 66%). Mass spectrometry (ESI positive ion): *m*/*z* 735.13 ([Co(c343ha)(tpa-(COOH)$_2$)]$^+$). Elemental analysis required for $C_{36}H_{40}Cl_2CoN_6O_{20}$: C, 42.96%, H, 4.01%, N, 8.35%. Found: C, 42.85%, H, 4.00%, N, 8.44%.

Synthesis of [Co(c343haH)(tpa(COOH)$_3$)](ClO$_4$)$_2$.2H$_2$O 9. The precipitate was collected by suction filtration to give a brown solid. This was dissolved in H_2O (70 mL), acidified to a pH of 4 with 1 M aqueous $HClO_4$, and then washed with 3 × 100 mL DCM. The aqueous fraction was evaporated to dryness, and the residue was washed with a small amount of ice-cold H_2O and excess Et_2O. The complex was recrystallized from hot (1:1) iPrOH:H_2O to give a brown solid (yield: 59%). Mass spectrometry (ESI positive ion): *m*/*z* 267.40 ([Co(c343ha)(tpaCOOH)$_3$]$^{2+}$ + Na^+). Elemental analysis required for $C_{37}H_{32}Cl_2CoN_6O_{20}$: C, 43.80%, H, 3.58%, N, 8.28%. Found: C, 43.33%, H, 3.59%, N, 8.35%.

Methods and Instrumentation. ^{1}H NMR spectra were collected at 300 K on a Bruker 300 MHz spectrometer using commercially available deuterated solvents. ^{1}H NMR spectra of complexes **7**, **8**, and **9** were recorded in MeOD or MeOD acidified to pH 3 by addition of 1 M DCl using a water suppression pulse program. TSP (3-

(trimethylsilyl)propionic acid) was used as an internal reference in D_2O. In all other solvents, isotopic impurities were used as internal reference signals. Mass spectrometry was performed using electrospray ionization using a Finnigan LCQ-8 spectrometer. Microanalysis (C, H, N) was conducted by Chemical & MicroAnalytical Services Pty Ltd., Campbell Microanalytical Laboratory at the University of Otago and by the Microanalytical Laboratories at the Australian National University.

pH Titration. pK_a determination using UV−vis spectroscopy was carried out by adjusting the pH of the solution of the compounds and measuring the UV−vis spectra. UV−visible spectra were measured at room temperature on a Cary 4E UV−visible spectrophotometer using a 1 cm ×1 cm quartz cuvette (Starna). Scans were run in absorption mode between 350 and 650 nm on freshly prepared 7×10^{-5} M solutions of the compounds in (1:50) MeOH:H_2O. A (1:50) MeOH:H_2O solution was used as the blank. The pH was adjusted using NaOH and HCl in (1:50) MeOH:H_2O and measured using a HI 991002 pH meter (Hanna Instruments). The absorbance at 475 nm was plotted as a function of pH.

Charges were calculated as %ionized = $100/(1 + 10^{(-(pH-pk_a))})$.

Fluorescence Spectra. Fluorescence measurements were performed using a Varian Cary Eclipse fluorescence spectrophotometer, with a 1 cm × 1 cm quartz cuvette (Starna). Scans were run at room temperature as 7×10^{-5} M solutions at pH 7.5 (adjusted with 1 M NaOH) in (1:50) MeOH:H_2O at 100 nm/min with excitation and emission slit widths of 2.5 nm. All solutions were prepared immediately prior to analysis. Emission scans were run between 400 and 600 nm using an excitation wavelength of 395 nm.

pH Dependent Fluorescence. pH-Dependent fluorescence of the compounds was carried out by adjusting the pH of the solutions of the compounds and measuring the fluorescence emission spectra in a similar manner to that described above. The pH was adjusted using 1 M NaOH and HCl in (1:50) MeOH:H_2O and measured using a HI 991002 pH meter (Hanna Instruments). The λ_{max} of the emission spectrum as a function of pH was plotted.

Reduction in Situ. Emission scans were collected between 450 and 600 nm with an excitation wavelength of 395 nm at regular time intervals over 70 h (every 30 min for the first 20 h then every 2 h for the second 50 h) on 7×10^{-5} M solutions in (1:50) MeOH:H_2O following the addition of 10 mol equiv of L-ascorbic acid. Similar measuring conditions to those described above were used. The measurements were repeated on identical solutions that had been deoxygenated by passing a stream of nitrogen through the solution for 10 min and tightly sealing the cuvette.

Electrochemistry. Electrochemical measurements were performed at room temperature using a BAS 100B/W electrochemical analyzer at a scan rate of 100 mV s^{-1} using a glassy carbon working electrode and a platinum auxiliary electrode. The experiments were performed at room temperature and were *iR* compensated. All samples were degassed with argon for at least 10 min prior to measurement.

Scans carried out in organic media were performed with 1 mM solutions in DMF with 0.1 M tetrapropylammonium perchlorate as the supporting electrolyte. A silver wire was used as a quasireference electrode, and the ferrocene/ferrocenium couple was used as an internal reference ($[Fe(\eta^5\text{-}C_5H_5)_2]^{0/+}$ = +0.72 V vs NHE in DMF at 25 °C).[44]

Scans carried out in aqueous media were performed with 1 mM solutions with 0.1 M sodium perchlorate as the supporting electrolyte. The silver | silver chloride reference electrode was used, and the scans were referenced to the Ag/AgCl couple (Ag/AgCl, KCl (saturated) = +0.198 vs NHE in H_2O at 25 °C).[45]

Cell Lines. DLD-1 human colon carcinoma cells were obtained from ATCC and used within 6 months of resuscitation. Cells were maintained in complete media which is Advanced DMEM (Invitrogen) supplemented with 2% FBS (Invitrogen) and 2 mM glutamine (Invitrogen) in a humidified environment at 37 °C and 5% CO_2. HRE-Eos DLD-1 cells[16] were maintained in complete media supplemented with 250 μg/mL Geneticin (Invitrogen).

Cytotoxicity Assays. Complexes tested were prepared as 1 mM aqueous solutions containing 2% DMSO immediately prior to the assay. Cytotoxicity was determined using the MTT assay as previously described.[46] 1×10^5 cells were seeded onto each well of flat-bottomed 96-well plates and allowed to attach overnight. Cobalt complex solutions were added to quadruplicate wells at concentrations spanning a 4-log range (final DMF concentrations were limited to 0.5%) and incubated for 72 h. MTT (1.0 mM) was added to each well and were incubated for a further 4 h. The culture medium was removed from each well, DMSO (150 μL) was added, the plate shaken for 5 s, and the absorbance measured immediately at 600 nm in a Victor^{3}V microplate reader (Perkin-Elmer). IC_{50} values were determined as the drug concentration that reduced the absorbance to 50% of that in untreated control wells. At least three independent experiments were performed for each compound with quadruplicate readings in each experiment.

Confocal Microscopy of pH Dependent Uptake of Complexes in Cell Monolayer. The pH of Leibovitz-15 media (Invitrogen) was adjusted to 6.0, 6.5, 7.0, 7.4, and 8.0 using 1 M HCl or 1 M NaOH and filter sterilized through MinisartCA 0.2 μm sterile filters (Sartorius Stedim). Cells were plated onto black, μ-clear 96-well plates (Greiner Bio-One) and grown to 40−60% confluence in normal growth media. The media was replaced with pH-adjusted L15 media, and the cells were treated with the compound and incubated for 4 h. The cells were washed several times with PBS, fresh medium added, and the cells immediately imaged. A heated stage (Linkam Scientific) was used to maintain the temperature at 37 °C during imaging. The pH of the medium was found not to change significantly after incubation at 37 °C for 24 h in a Petri dish in the absence of cells.

Confocal fluorescence microscopy was performed using a Nikon Eclipse TE200 inverted fluorescence microscope and a Nikon Plan Fluor 40×/NA 0.75 DIC M air objective lens. Confocal images were collected using a Nikon DE-Eclipse microscope C1 and a Coherent Radius 405−25 optically pumped semiconductor laser system. The emission range was 433−467 nm. A scan rate of 15 ms/pixel was used for all images, and an average of 4 scans per image was collected. To compare the fluorescence intensities, the same laser power was used for all images. At least three images were taken per slide and repeated on at least three different occasions.

Quantification of the fluorescence intensity was carried out using ImageJ by drawing a 20 um^2 square over a representative portion of the image and measuring the integrated fluorescence intensity. Measurements were taken from at least five different images in each treatment group.

Cobalt Uptake of Complexes in Cell Monolayer. Four million DLD-1 cells in 6 mL of DMEM of were seeded in a 6 cm dish and allowed to adhere overnight. The media was replaced and the cells treated with 30 μM of the complexes in DMSO (final DMSO concentration = 0.3%). Following incubation for 4 h, the media was removed, the cells trypsinized, and 5 mL of PBS solution added. The cells were centrifuged at 2000 rpm for 4 min, the supernatant removed, and the process repeated three times. The pellet was then resuspended in 0.5 mL of PBS solution.

Cobalt concentrations were determined using ICP-MS by the National Measurements Institute, Pymble, NSW, Australia. Samples were digested with 15 M nitric acid prior to analysis. Cellular concentrations of cobalt were reported per mg of protein. Biorad protein assay dye was diluted 5-fold with double-distilled water, and 200 μL of the diluted reagent was then added to each well of a 96-well plate. Using 1 mg/mL solution of bovine serum albumin in PBS, protein standards of concentrations 500, 250, 125, 62.5, 31.3, and 15.6 μg/mL were prepared. Cellular samples were diluted by a factor of 10 before a 10 μL aliquot was added to each well containing the diluted dye reagent. The protein/dye mixtures were then shaken for 15 min, and the absorbance at 620 nm determined using a Victor^{3}V microplate reader (Perkin-Elmer). All analyses were performed in triplicate.

Confocal Microscopy of Spheroids. Spheroids were formed by plating 100 μL of a 2.5×10^5 cells/mL single cell suspension of DLD-1 onto agarose (sterile, 0.75% (w/v) in PBS) coated 96-well plates. They were allowed to aggregate for 5 days without motion, resulting in the formation of single spheroid per well.[36] Spheroids of HRE-Eos DLD-1 were grown in a similar manner in complete media supplemented with

dx.doi.org/10.1021/jm3014713 | J. Med. Chem. 2012, 55, 11013−11021

Geneticin (Invitrogen) (5 mg in 10 mL). On day 5, the spheroids were treated with 10 μM of compound (in up to 2% DMSO) for 4 h, washed with PBS, then replaced in media in black, μ-clear 96-well imaging plates (Greiner Bio-One) to be imaged. A heated stage (Linkam Scientific) was used to maintain the temperature at 37 °C during imaging. The HRE-Eos DLD-1 cells expressed the Eos photoconvertible green fluorescent protein when they were experiencing hypoxia.[16] The Eos protein was photoconverted to the red fluorescent form of the protein by exposing the spheroids to UV light for 1 min prior to imaging.

Confocal fluorescence microscopy was performed using a Nikon Eclipse TE200 inverted fluorescence microscope and a Nikon Plan Fluor 10×/NA 0.3 DIC objective lens. Confocal images were collected using a Nikon DE-Eclipse microscope C1 and a Coherent Radius 405−25 optically pumped semiconductor laser systems and a Melles Griot yellow 85-YCA025 561−10.5 diode-pumped solid state laser. The emission ranges were 433−467 nm and >580 nm, respectively. A scan rate of 15 ms/pixel was used for all images and an average of four scans per image was collected. At least three spheroids were imaged on each occasion, and the experiment was repeated on at least three different occasions.

Quantification of the fluorescence intensity was carried out using ImageJ by drawing a 350 μm circle in the middle of the spheroid and measuring the integrated fluorescence intensity. Measurements were taken from at least six different spheroids in each treatment group. Statistical analysis was performed using the unpaired t test. *$P < 0.005$ and **$P < 0.001$ compared to the preceding treatment group.

■ ASSOCIATED CONTENT

Ⓢ Supporting Information

^{1}H NMR spectra; pK_a determination of **1**, **7**, **8**, and **9**; pH-dependence of the fluorophore and the complexes; 72 h cytotoxicity (IC_{50}) of fluorophore complexes in DLD-1 human colon carcinoma cells. This material is available free of charge via the Internet at http://pubs.acs.org

■ AUTHOR INFORMATION

Corresponding Author

*For N.S.B.: phone, +61 2 9351 4233; fax, +61 2 9351 3329; E-mail, nicole.bryce@sydney.edu.au. For T.W.H.: phone, +61 2 9351 3320; fax, +61 2 9351 3329; E-mail, trevor.hambley@sydney.edu.au.

Author Contributions

The manuscript was written through contributions of all authors. All authors have given approval to the final version of the manuscript.

Notes

The authors declare no competing financial interest.

■ ACKNOWLEDGMENTS

We acknowledge scientific and technical input and support from the Australian Microscopy & Microanalysis Research Facility (AMMRF) node at the University of Sydney. We thank the Australian Research Council for support through grants DP0773953 and DP110100461 and the Swiss National Science Foundation for a postdoctoral fellowship (A.K.R.).

■ ABBREVIATIONS USED

$ahaH_2$, acetohydroxamic acid; c343, coumarin-343; c343haH, coumarin-343-hydroxamic acid; cyclam, 1,4,8,11-tetraazacyclotetradecane; DMEM, Dulbecco's Modified Eagle's Medium; DMSO, dimethylsulfoxide; mmst, Marimastat; tpa, tris(2-methylpyridine)amine; $tpa(COOH)_1$, 6-((bis(pyridin-2-ylmethyl)amino)methyl)nicotinic acid; $tpa(COOH)_2$, 6,6′-(pyridine-2-ylmethylazanediyl)bis(methylene)dinicotinic acid; $tpa(COOH)_3$, 6,6′,6″-nitrolotris(methylene)trinicotinic acid; TSP, 3-(trimethylsilyl)propionic acid

■ REFERENCES

(1) Zeman, E. M.; Brown, J. M.; Lemmon, M. J.; Hirst, V. K.; Lee, W. W. SR-4233: a new bioreductive agent with high selective toxicity for hypoxic mammalian cells. *Int. J. Radiat. Oncol.* **1986**, *12*, 1239−1242.

(2) Raghunand, N.; He, X.; van Sluis, R.; Mahoney, B.; Baggett, B.; Taylor, C. W.; Paine-Murrieta, G.; Roe, D.; Bhujwalla, Z. M.; Gillies, R. J. Enhancement of chemotherapy by manipulation of tumour pH. *Br. J. Cancer* **1999**, *80*, 1005−1011.

(3) Wilson, W. R.; Hay, M. P. Targeting hypoxia in cancer therapy. *Nature Rev. Cancer* **2011**, *11*, 393−410.

(4) Denny, W. A. Hypoxia-activated prodrugs in cancer therapy: progress to the clinic. *Future Oncol.* **2010**, *6*, 419−428.

(5) DeClerck, K.; Elble, R. C. The role of hypoxia and acidosis in promoting metastasis and resistance to chemotherapy. *Front. Biosci.* **2010**, *15*, 213−225.

(6) Gort, E. H.; Groot, A. J.; van der Wall, E.; van Diest, P. J.; Vooijs, M. A. Hypoxic regulation of metastasis via hypoxia-inducible factors. *Curr. Mol. Med.* **2008**, *8*, 60−67.

(7) Boucher, Y.; Baxter, L. T.; Jain, R. K. Interstitial pressure gradients in tissue-isolated and subcutaneous tumors: implications for therapy. *Cancer Res.* **1990**, *50*, 4478−4484.

(8) Chauhan, V. P.; Stylianopoulos, T.; Boucher, Y.; Jain, R. K. Delivery of molecular and nanoscale medicine to tumors: transport barriers and strategies. *Annu. Rev. Chem. Biomol. Eng.* **2011**, *2*, 281−298.

(9) Minchinton, A. I.; Tannock, I. F. Drug penetration in solid tumours. *Nature Rev. Cancer* **2006**, *6*, 583−592.

(10) Milbank, J. B.; Stevenson, R. J.; Ware, D. C.; Chang, J. Y.; Tercel, M.; Ahn, G. O.; Wilson, W. R.; Denny, W. A. Synthesis and evaluation of stable bidentate transition metal complexes of 1-(chloromethyl)-5-hydroxy-3-(5,6,7-trimethoxyindol-2-ylcarbonyl)-2,3-dihydro-1*H*-pyrrolo[3,2-*f*]quinoline (*seco*-6-azaCBI-TMI) as hypoxia selective cytotoxins. *J. Med. Chem.* **2009**, *52*, 6822−6834.

(11) Ware, D. C.; Brothers, P. J.; Clark, G. R.; Denny, W. A.; Palmer, B. D.; Wilson, W. R. Synthesis, structures and hypoxia-selective cytotoxicity of cobalt(III) complexes containing tridentate amine and nitrogen mustard ligands. *Dalton Trans.* **2000**, *6*, 925−932.

(12) Teicher, B. A.; Abrams, M. J.; Rosbe, K. W.; Herman, T. S. Cytotoxicity, radiosensitization, antitumor activity, and interaction with hyperthermia of a Co(III) mustard complex. *Cancer Res.* **1990**, *50*, 6971−6975.

(13) Ware, D. C.; Wilson, W. R.; Denny, W. A.; Richard, C. E. F. Design and synthesis of cobalt(III) nitrogen mustard complexes as hypoxia selective cytotoxins. The X-ray crystal structure of bis(3-chloropentane-2,4-dionato)(*RS*-*N*,*N*′-bis(2-chloroethyl)-ethylenediamine)cobalt(III) perchlorate, $[Co(Clacac)_2(bce)]ClO_4$. *Chem. Commun.* **1991**, *17*, 1171−1173.

(14) Ware, D. C.; Palmer, B. D.; Wilson, W. R.; Denny, W. A. Hypoxia-selective antitumor agents. 7. Metal complexes of aliphatic mustards as a new class of hypoxia-selective cytotoxins. Synthesis and evaluation of cobalt(III) complexes of bidentate mustards. *J. Med. Chem.* **1993**, *36*, 1839−1846.

(15) Failes, T. W.; Hambley, T. W. Models of hypoxia activated prodrugs: Co(III) complexes of hydroxamic acids. *Dalton Trans.* **2006**, *6*, 1895−1901.

(16) Kim, B. J.; Hambley, T. W.; Bryce, N. S. Visualising the hypoxia selectivity of cobalt(III) prodrugs. *Chem. Sci.* **2011**, *2*, 2135−2142.

(17) Yamamoto, N.; Danos, S.; Bonnitcha, P. D.; Failes, T. W.; New, E. J.; Hambley, T. W. Cellular uptake and distribution of cobalt complexes of fluorescent ligands. *J. Biol. Inorg. Chem.* **2008**, *13*, 861−871.

(18) Whittaker, M.; Floyd, C. D.; Brown, P.; Gearing, A. J. H. Design and Therapeutic Application of Matrix Metalloproteinase Inhibitors. *Chem. Rev.* **1999**, *99*, 2735−2776.

(19) Failes, T. W.; Cullinane, C.; Diakos, C. I.; Yamamoto, N.; Lyons, G. J.; Hambley, T. W. Studies of a Co(III) complex of the

MMP inhibitor marimastat: a potential hypoxia activated prodrug. *Chem.—Eur. J.* **2007**, *13*, 2974−2982.
(20) Gallagher, F. A.; Kettunen, M. I.; Day, S. E.; Hu, D.-E.; Ardenkjaer-Larsen, J. H.; in't Zandt, R.; Jensen, P. R.; Karlsson, M.; Golman, K.; Lerche, M. H.; Brindle, K. M. Magnetic resonance imaging of pH in vivo using hyperpolarized 13C-labelled bicarbonate. *Nature* **2008**, *453*, 940−943.
(21) Gerweck, L. E.; Vijayappa, S.; Kozin, S. Tumor pH controls the in vivo efficacy of weak acid and base chemotherapeutics. *Mol. Cancer Ther.* **2006**, *5*, 1275−1279.
(22) Gillies, R. J.; Raghunand, N.; Garcia-Martin, M. L.; Gatenby, R. A. pH imaging. A review of pH measurement methods and applications in cancers. *IEEE Eng. Med. Biol.* **2004**, *23*, 57−64.
(23) Gillies, R. J.; Raghunand, N.; Karczmar, G. S.; Bhujwalla, Z. M. MRI of the tumor microenvironment. *J. Magn. Reson. Imaging* **2002**, *16*, 430−450.
(24) Gerweck, L. E.; Kozin, S. V.; Stocks, S. J. The pH partition theory predicts the accumulation and toxicity of doxorubicin in normal and low-pH-adapted cells. *Br. J. Cancer* **1999**, *79*, 838−842.
(25) Raghunand, N.; Gillies, R. J. pH and drug resistance in tumors. *Drug Resist. Update* **2000**, *3*, 39−47.
(26) Mikkelsen, R. B.; Asher, C.; Hicks, T. Extracellular pH, transmembrane distribution and cytotoxicity of chlorambucil. *Biochem. Pharmacol.* **1985**, *34*, 2531−2534.
(27) Breiner, B.; Kaya, K.; Roy, S.; Yang, W. Y.; Alabugin, I. V. Hybrids of amino acids and acetylenic DNA-photocleavers: optimizing efficiency and selectivity for cancer phototherapy. *Org. Biomol. Chem.* **2012**, *10*, 3974−3987.
(28) Yang, W. Y.; Roy, S.; Phrathep, B.; Rengert, Z.; Kenworthy, R.; Zorio, D. A.; Alabugin, I. V. Engineering pH-gated transitions for selective and efficient double-strand DNA photocleavage in hypoxic tumors. *J. Med. Chem.* **2011**, *54*, 8501−8516.
(29) Lu, G. L.; Stevenson, R. J.; Chang, J. Y.; Brothers, P. J.; Ware, D. C.; Wilson, W. R.; Denny, W. A.; Tercel, M. *N*-Alkylated cyclen cobalt(III) complexes of 1-(chloromethyl)-3-(5,6,7-trimethoxyindol-2-ylcarbonyl)-2,3-dihydro-1*H*-pyrrolo[3, 2-*f*]quinolin-5-ol DNA alkylating agent as hypoxia-activated prodrugs. *Bioorgan. Med. Chem.* **2011**, *19*, 4861−4867.
(30) Green, R. W.; Tong, H. K. Constitution of the pyridine monocarboxylic acids in their isoelectric forms. *J. Am. Chem. Soc.* **1956**, *78*, 4896−4900.
(31) Schwarzenbach, G.; Schwarzenbach, K. Hydroxamate complexes. I. The stabilities of the iron(III) complexes of simple hydroxamic acids and desferriferrioxamin B. *Helv. Chim. Acta* **1963**, *46*, 1390−1400.
(32) Mascharak, P. K. Structural and functional models of nitrile hydratase. *Coord. Chem. Rev.* **2002**, *225*, 201−214.
(33) Wojtkowiak, J. W.; Verduzco, D.; Schramm, K. J.; Gillies, R. J. Drug resistance and cellular adaptation to tumor acidic pH microenvironment. *Mol. Pharmaceutics* **2011**, *8*, 2032−2038.
(34) Bonny, C., Coquoz, D. and Chen, J. Conjugates with enhanced cell uptake activity. EP patent 2004−269341656951, 2006.
(35) Aguilera, T. A.; Olson, E. S.; Timmers, M. M.; Jiang, T.; Tsien, R. Y. Systemic in vivo distribution of activatable cell penetrating peptides is superior to that of cell penetrating peptides. *Integr. Biol.* **2009**, *1*, 371−381.
(36) Bryce, N. S.; Zhang, J. Z.; Whan, R. M.; Yamamoto, N.; Hambley, T. W. Accumulation of an anthraquinone and its platinum complexes in cancer cell spheroids: the effect of charge on drug distribution in solid tumour models. *Chem. Commun.* **2009**, *19*, 2673−2675.
(37) Zhang, J. Z.; Bryce, N. S.; Siegele, R.; Carter, E. A.; Paterson, D.; de Jonge, M. D.; Howard, D. L.; Ryan, C. G.; Hambley, T. W. The use of spectroscopic imaging and mapping techniques in the characterisation and study of DLD-1 cell spheroid tumour models. *Integr. Biol.* **2012**, *4*, 1072−1080.
(38) Robey, R. W.; Chakraborty, A. R.; Basseville, A.; Luchenko, V.; Bahr, J.; Zhan, Z.; Bates, S. E. Histone deacetylase inhibitors: emerging mechanisms of resistance. *Mol. Pharmaceutics* **2011**, *8*, 2021−2031.
(39) Anderegg, G.; Wenk, F. Pyridine derivatives as complexing agents. VIII. Preparation of a new quadridentate and a new hexadentate ligand. *Helv. Chim. Acta* **1967**, *50*, 2330−2332.
(40) Chong, H.-S.; Torti, S. V.; Ma, R.; Torti, F. M.; Brechbiel, M. W. Synthesis and potent antitumor activities of novel 1,3,5-*cis*,*cis*-triaminocyclohexane *N*-pyridyl derivatives. *J. Med. Chem.* **2004**, *47*, 5230−5234.
(41) Yamaguchi, M.; Kumano, T.; Masui, D.; Yamagishi, T. Photoassisted oxygenation of alkane catalyzed by ruthenium complexes using 2,6-dichloropyridine *N*-oxide under visible light irradiation. *Chem. Commun.* **2004**, *10*, 798−799.
(42) Tyeklar, Z.; Jacobson, R. R.; Wei, N.; Murthy, N. N.; Zubieta, J.; Karlin, K. D. Reversible reaction of dioxygen (and carbon monoxide) with a copper(I) complex. X-ray structures of relevant mononuclear Cu(I) precursor adducts and the *trans*-(μ-1,2-peroxo)dicopper(II) product. *J. Am. Chem. Soc.* **1993**, *115*, 2677−2689.
(43) Yamaguchi, M.; Kousaka, H.; Izawa, S.; Ichii, Y.; Kumano, T.; Masui, D.; Yamagishi, T. Syntheses, characterization, and catalytic ability in alkane oxygenation of chloro(dimethyl sulfoxide)ruthenium(II) complexes with tris(2-pyridylmethyl)amine and its derivatives. *Inorg. Chem.* **2006**, *45*, 8342−8354.
(44) Barrette, W. C., Jr.; Johnson, H. W., Jr.; Sawyer, D. T. Voltammetric evaluation of the effective acidities (pK_a') for Broensted acids in aprotic solvents. *Anal. Chem.* **1984**, *56*, 1890−1898.
(45) Meites, L., *Handbook of Analytical Chemistry*; McGraw Hill: New York, 1963; p 1788.
(46) Carmichael, J.; DeGraff, W. G.; Gazdar, A. F.; Minna, J. D.; Mitchell, J. B. Evaluation of a tetrazolium-based semiautomated colorimetric assay: assessment of chemosensitivity testing. *Cancer Res.* **1987**, *47*, 936−942.